Electronic transport properties of electron- and hole-doped semiconducting $C1_b$ Heusler compounds: $NiTi_{1-x}M_xSn$ (M=Sc, V)

Siham Ouardi, Gerhard H. Fecher,* Benjamin Balke, Xenia Kozina, Gregory Stryganyuk, and Claudia Felser
Institut für Anorganische und Analytische Chemie, Johannes Gutenberg-Universität, 55099 Mainz, Germany

Stephan Lowitzer, Diemo Ködderitzsch, and Hubert Ebert
Department Chemie, Physikalische Chemie, Ludwig-Maximilians-Universität, 81377 München, Germany

Eiji Ikenaga
Japan Synchrotron Radiation Research Institute, SPring-8, Hyogo 679-5198, Japan

(Received 20 April 2010; revised manuscript received 17 June 2010; published 11 August 2010)

The substitutional series of Heusler compounds $NiTi_{1-x}M_xSn$ (where M=Sc,V and $0<x\leq 0.2$) were synthesized and investigated with respect to their electronic structure and transport properties. The results show the possibility to create *n*-type and *p*-type thermoelectrics within one Heusler compound. The electronic structure and transport properties were calculated by all-electron *ab initio* methods and compared to the measurements. Hard x-ray photoelectron spectroscopy was carried out and the results are compared to the calculated electronic structure. Pure NiTiSn exhibits massive "in gap" states containing about 0.1 electrons per cell. The comparison of calculations, x-ray diffraction, and photoemission reveals that Ti atoms swapped into the vacant site are responsible for these states. The carrier concentration and temperature dependence of electrical conductivity, Seebeck coefficient, and thermal conductivity were investigated in the range from 10 to 300 K. The experimentally determined electronic structure and transport measurements agree well with the calculations. The sign of the Seebeck coefficient changes from negative for V to positive for Sc substitution. The high *n*-type and low *p*-type power factors are explained by differences in the chemical-disorder scattering-induced electric resistivity. Major differences appear because *p*-type doping (Sc) creates holes in the triply degenerate valence band at Γ whereas *n*-type doping (V) fills electrons in the single conduction band above the indirect gap at *X* what is typical for all semiconducting transition-metal-based Heusler compounds with $C1_b$ structure.

DOI: 10.1103/PhysRevB.82.085108 PACS number(s): 31.15.A−, 71.23.−k, 72.15.Jf

I. INTRODUCTION

Heusler compounds are ternary intermetallics consisting of two transition metals and one main group element. The Heusler compounds with a 1:1:1 composition crystallize in the cubic MgAgAs-type structure ($F\bar{4}3m, C1_b$).[1,2] Most of those with 18 valence electrons in the primitive cell are expected to be semiconducting.[3] They are considered to be promising thermoelectric materials because of their potential role in the realization of environmentally friendly technology (see Ref. 4 for a recent review).

The compounds of the general formula Ni*M*Sn (M=Ti,Zr,Hf) have 18 valence electrons. They were reported to exhibit unusual transport and optical properties because of the band gap or pseudogap at the Fermi energy. Sakurada and Shutoh[5,6] reported a high figure of merit of 1.5 at 700 K for Sb-doped $NiTi_{0.50}Zr_{0.25}Hf_{.25}Sn$, which is one of the highest values for Heusler compounds at that temperature. A variety of substitutions in Ni*M*Sn with other main-group metals as well as transition metals have been made for further optimization of the thermoelectric performance.[4] For example, doping on the *M* and Ni sites causes mass fluctuation disorder that may lead to a reduction in thermal conductivity[6–10] while doping on the Sn site provides charge carriers.[7,10] Numerous Heusler alloys have been investigated focusing on their high-temperature thermoelectric properties. The majority of these compounds are *n*-type thermoelectric materials. On the other hand, efficient *p*-type materials based on Heusler compounds that operate at high temperatures are rare.

In order to achieve the best performance of thermoelectric modules the *n*- and *p*-type materials to be used should be designed to exhibit similar chemical and physical properties.[11] This can be easily realized when starting from the same material, here the Heusler compound NiTiSn. Yang[12] evaluated theoretically the thermoelectric-related electrical transport properties of several Heusler compounds, they calculated the maximum power factors and the corresponding optimal *n*- or *p*-type doping levels, which can provide guidance to experimental work. Horyn' *et al.*[13] investigated the effect of a partial substitution of Ti and Zr by Sc on the thermoelectric properties of Ni*M*Sn-based compounds and obtained at room temperature a fairly high positive Seebeck coefficient of about 121 μV/K with 5% Sc substitution of Zr. Miyamoto *et al.*[14] studied the electronic structures of the Heusler compounds Ni*M*Sn by means of photoelectron spectroscopy. They observed "in gap" states close to the Fermi edge and suggested that these electronic states are mainly created by chemical disorder, which could be the key to control the thermoelectric properties.

In the commonly used one-parabolic-band approaches *n*- or *p*-type doping lead to rather similar results, just with opposite signs for the Seebeck coefficient. The situation in practical materials is more difficult. Depleting the valence or filling the conduction band acts on electronic states with

 ©2010 The American Physical Society

rather different characters. It will be shown that the effect of doping shows a completely different impact for the NiTiSn compounds when comparing *n*- and *p*-type substitutions. To explain the different effects on the conductivity a new approach is used that combines the coherent potential approximation and calculation of the impurity-scattering resistivity for the multielement case. In the present study, the electronic structure and transport properties of the series $NiTi_{1-x}M_xSn$ (where $M=Sc,V$ and $0<x\leq 0.2$) were calculated by *ab initio* methods. The series was synthesized and the structure was determined by x-ray diffraction (XRD). The transport properties were investigated and the results are compared to the calculated properties. Hard x-ray photoelectron spectroscopy (HAXPES) was performed on the compounds to experimentally determine the valence states and to compare them to the calculated electronic structure.

II. DETAILS OF THE CALCULATIONS

The electronic structure and transport properties were calculated by all-electron *ab initio* methods. The full-potential linearized augmented plane-wave method as implemented in WIEN2k (Ref. 15) in combination with a modified version of BOLTZTRAP (Ref. 16) has been used for ordered, pure 1:1:1 compounds (for details see Refs. 17 and 18). If not noted otherwise, the exchange-correlation functional was taken within the generalized gradient approximation (GGA) in the parametrization of Perdew-Burke-Enzerhof (PBE).[19] A $(31\times 31\times 31)$ point mesh was used resulting in 816 k points in the irreducible wedge of the Brillouin zone. The energy convergence criterion was set to 10^{-5} Ry and simultaneously the criterion for charge convergence to $10^{-3}e^-$. The muffin-tin radii were set to $2.4a_B$ for the transition metals and $2.25a_B$ for the main group element (Bohr's radius: $a_B=0.5291772$ Å). For the calculation of the transport properties the tetrahedron method and energy steps of $\approx 0.16\times 10^{-04}$ Ry were used for integration. Relaxed lattice parameters were used in all calculations, the optimization of the volume resulted in $a=5.9534$ Å for NiTiSn. Typical for the use of GGA, this value is slightly larger (0.6%) compared to the one found from experiments. This is not a critical issue as the band gap is rather stable against variation in a independent of the used functional (see below).

The electronic-structure calculations of the substitutionally disordered $NiTi_{1-x}M_xSn$ (where $M=Sc,V$ and $0<x\leq 0.2$) have been performed by means of the fully relativistic Korringa-Kohn-Rostoker (KKR) method in combination with the coherent potential approximation (CPA) as implemented in the MUNICH-SPRKKR program package.[20] The k-integration mesh was set to a size of $(22\times 22\times 22)$ during the self-consistent cycles. The gradient correction of the PBE functional was switched off for the vacant site to avoid numerical instabilities caused by low charge densities.

The CPA allows electronic-structure calculations for systems with random distribution of the atoms as is here the case where M substitutes partially Ti. For the substitutional compounds, the CPA method has been used to model the statistic distribution of the atoms on the M site and the Ti atoms on a common site of the $C1_b$ crystalline structure. The Ni atoms are placed on the 4a Wyckoff position, the Ti atoms are placed together with the M atoms on the 4c position, and the main group element Sn is finally placed on the 4d position of the cell with $F\bar{4}3m$ symmetry (space group 216). The swap-type disordered NiTiSn (for example, $Ni_{1-x}Vc_xTiSn$) compound was also treated using the CPA method by placing a fraction of x vacancies (Vc) on regular sites and simultaneously the swapped part $(1-x)$ on the 4b Wyckoff position.

The conductivity of the compounds with random substitution was calculate using the Kubo-Greenwood linear-response formalism as described in Ref. 21 including vertex corrections.[22] The original formulation[22] was for the case of one site per cell and is extended in the present work to include primitive cells with a basis that contains several different sites. The chemical-disorder scattering resistivity of $NiTi_{1-x}M_xSn$ was calculated using an enlarged $(92\times 92\times 92)$ k mesh.

The transport properties discussed in the following depend, indeed, critically on the size of the band gap. It is often noted that the local-density approximation underestimates the band gaps of semiconductors and insulators (for a recent discussion see Ref. 23). Very often, specialized functionals [for example, the Engel-Vosko (EV) GGA functional (Ref. 24)] or hybrid functionals including Hartree-Fock exchange [for example, Becke's B3LYP (Ref. 25)] give better values for the band gaps if applied to *sp*-element-based semiconductors, likewise Ge (0.17 eV with PBE, 0.65 eV with EV, and 0.78 eV in experiments) or GaAs [0.48 eV (PBE), 1.04 eV (EV), and 1.5 eV (exp)]. To check for influences of the exchange-correlation functional, the electronic structure of NiTiSn was also calculated using the local spin density approximation (LSDA),[26] EV-GGA,[24] and the PBEsol (Ref. 27) functionals. Surprisingly, the size of the band gap stayed stable within less than 100 meV without remarkable changes in the band structure. This points to a fundamental difference in the description of *d*-element-based Heusler semiconductors compared to the *sp*-element materials. Obviously, the band gap of the *d*-element semiconductors investigated here is much less influenced by the choice of the functional as compared to *sp*-type semiconductors.

III. EXPERIMENTAL DETAILS

The series $NiTi_{1-x}M_xSn$ ($M=Sc,V$ and $x=0,\ldots,0.1$) was prepared by arc melting using a mixture of stoichiometric amounts of the elements. To ensure the homogeneity of the samples they were remelted several times. The as-cast samples were subsequently annealed at 950 °C for 72 h followed by quenching in ice water in order to improve the crystalline order. The existence of a single and compositionally homogeneous phase was verified by x-ray powder diffraction using Mo $K\alpha$ radiation. The determination of the lattice parameters and the crystal-structure refinements were performed using the Rietveld method.

For the transport measurement bars of $(2\times 2\times 8)$ mm^3 were cut from the ingots and polished on each side. The measurements of the Seebeck coefficient, thermal conductivity, and resistivity were performed by means of a physical properties measurement system (Quantum Design Model:

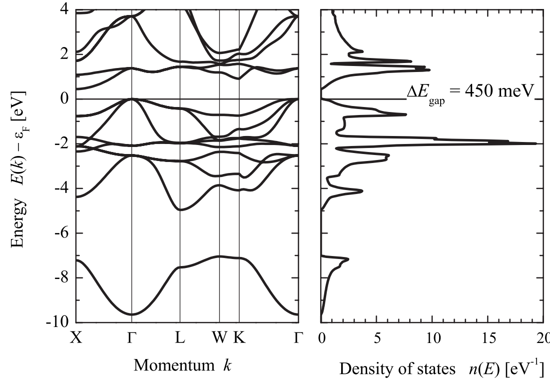

FIG. 1. Electronic structure of NiTiSn.

6000; supported by LOT, Germany). The temperature was varied from 10 K to room temperature. The measurements were performed at a residual pressure of about 9.0×10^{-5} mbar in the chamber.

The HAXPES experiments were performed at the undulator beamline BL47XU of SPring-8 (Hyogo, Japan). The photon energy was fixed at 7.9382 keV using a Si(111) double crystal monochromator and a Si(444) channel-cut postmonochromator. The photoemitted electrons were analyzed for their kinetic energy and detected by a hemispherical analyzer (VG Scienta R4000). The overall energy resolution (monochromator plus analyzer) was set to 250 meV, as verified by low-temperature spectra of the Au valence band at the Fermi energy (ϵ_F). Additionally, spectra close to the Fermi energy were taken with a resolution of 150 meV. The angle between the electron spectrometer and photon propagation is fixed at 90° in all experiments. A near normal emission ($\theta=2°$) detection angle was used resulting in an angle of photon incidence of $\alpha=88°$. For the HAXPES investigations, the sample bars were fractured *in situ*. This assures that the samples are free of oxygen contamination. The measurements were taken at sample temperatures of 20 and 300 K.

IV. RESULTS AND DISCUSSION

A. Electronic structure and transport

Figure 1 shows the calculated band structure and the density of states of NiTiSn. The compound is a semiconductor with an indirect gap. The valence-band maximum appears at Γ and the conduction-band minimum at X. The band gap has a size of $\Delta E_{gap}=0.45$ eV. The optical gap at Γ is considerably larger ($\Delta E_{\Gamma}=1.38$ eV).

The electronic structure exhibits at 5–8 eV below the Fermi energy the typical sp hybridization gap that separates the low-lying $a_1(s)$ from the $t_1(p)$ bands. The high density of states at about −2 eV emerges mainly from Ni d states. The high density of states at −0.7 eV arises mainly from Ni d states with e symmetry. Most important for the transport properties, the states at both band edges are due to Ti d states with t_2 symmetry. From the band structure shown in Fig. 1 it is obvious that electron (n) or hole (p) doping will have rather different results. It is easily seen that p-type doping creates holes in the triply degenerate valence band at Γ

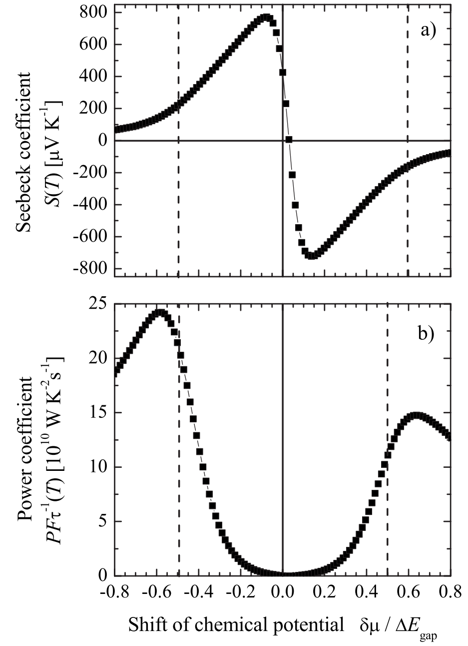

FIG. 2. Calculated Seebeck and power coefficients of NiTiSn. The shift of the chemical potential is given with respect to the size of the gap. The valence and conduction band extrema are marked by dashed lines ($T=300$ K).

whereas the situation is completely different for n-type doping that fills electrons into the single conduction band above the indirect gap at X.

Starting from the calculated electronic structure, the transport properties were calculated using Boltzmann transport theory.[28] Doping the semiconducting materials by electrons or holes will change the transport properties. The doping will cause the chemical potential to change its position. At high-doping levels it will shift into the valence (hole doping) or conduction (electron doping) band. Figure 2 shows the calculated Seebeck and power coefficients as function of the position of the chemical potential. The calculations were performed for $T=300$ K. It is assumed that the shift $\delta\mu=0$ corresponds to the middle of the band gap at $T=0$. In Refs. 29 and 30 the calculated Boltzmann transport quantities were reported as a function of the chemical potential and temperature for much higher doping level using the same method. The results agree with the here reported values for low doping that close the gap in the considered range of substitution.

The Seebeck coefficient exhibits the typical semiconductor behavior under doping, it is positive for hole and negative for electron doping. It is largest for small shifts of the chemical potential from the original position. At 300 K it is already slightly positive in the middle of the band gap, the reason is the shift of the chemical potential with temperature $\mu=\mu(T)$ to ensure charge neutrality of the system when no voltage is applied. At 300 K the shift amounts to $\delta\mu \approx 13$ meV. The size and direction of the shift depend on the shape of the valence and conduction bands.

Figure 3 shows the temperature dependence of the chemical potential and its effect on the Seebeck coefficient of the undoped material. $\delta\mu$ was also calculated for low electron or hole doping ($10^{-6}, 10^{-3}$) with hypothetical impurity states lo-

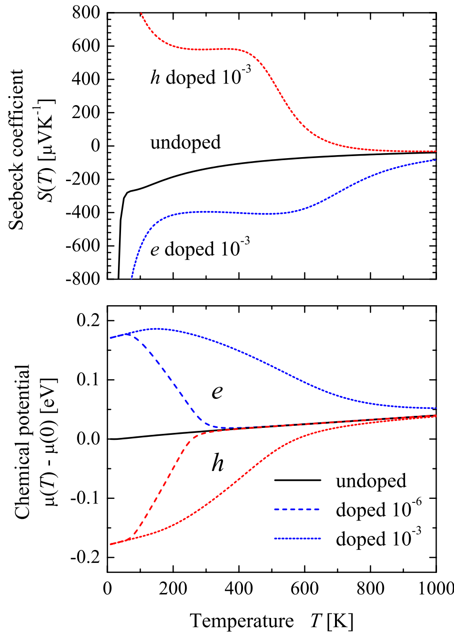

FIG. 3. (Color online) Seebeck coefficient and chemical potential of NiTiSn. The shift of the chemical potential was calculated for pure as well as electron- and hole-doped NiTiSn (*e* and *h* assign electron and hole doping, respectively).

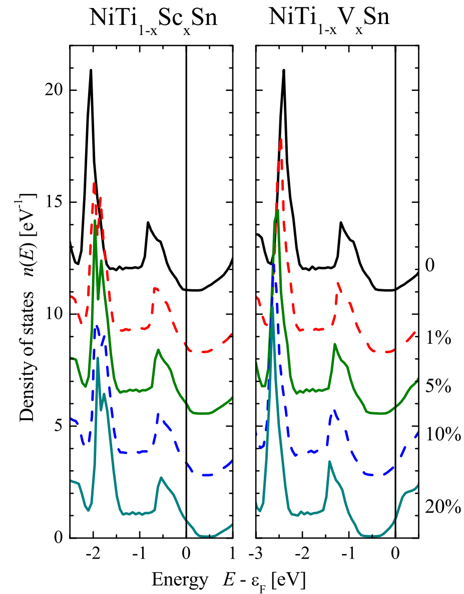

FIG. 4. (Color online) Density of states of M=Sc- and V-substituted $NiTi_{1-x}M_xSn$. For better comparison, the Fermi energy (ϵ_F) of the pure NiTiSn was set to the valence-band maximum in the case of Sc substitution and to the conduction-band minimum for V substitution.

cated close to the band edges (±50 meV). It is seen that the chemical potential is pinned at the impurity states at very low temperature. In the high-temperature limit the chemical potential goes over into the one of the pure semiconductor, depending on the degree of doping.

For applications, the power factor $PF=S^2\sigma$ is more interesting than the Seebeck coefficient alone. The power coefficient, as shown in Fig. 2(b), is defined here by the power factor divided by the relaxation time τ. The reason for this is that the calculations deliver σ/τ rather than directly the pure conductivity. The largest power coefficient appears for hole doping when the chemical potential is already shifted slightly outside of the band gap into the valence band. The maximum for electron doping is smaller and also appears when μ is slightly shifted outside of the gap. The reason for this is in both cases the high conductivity when the compound goes over into the completely metallic state. From the integrated density of states it is estimated that the maxima of the power coefficient are reached at an electron or hole doping of about 1.1% or 1.4%, respectively.

Substituting Ti by V or Sc will act as electron or hole doping, respectively. The difference in the number of valence electrons is in both cases one, such that a substitution by an amount x changes the electron concentration also by $\pm x$. At high substitution levels in the order of several percent it is, however, not clear *a priori* that the electronic structure stays unchanged and only the chemical potential or Fermi energy is shifted. Therefore, the electronic structure was also calculated for substituted compounds using values up to $x=0.2$.

The density of states of M=Sc or V substituted $NiTi_{1-x}M_xSn$ is shown in Fig. 4. The band gap is conserved upon substitution up to the 20% level for both elements, Sc and V. Overall, the shape of the density of states stays rather unaffected up to $x=0.2$. The main effect of the substitution is the shift of the Fermi energy such that the compound becomes metallic. Other than in the earlier studies on Fe-substituted $CoTi_{1-x}M'_xSb$ (M'=Mn,Fe) (Refs. 31 and 32) a magnetic ground state was not found by the calculations. One reason might be the much higher electron concentration (4 per substituted Fe) compared to the case studied here or the strong tendency of Mn to form localized moments.

B. Experimental results

Based on the theoretical findings, the series $NiTi_{1-x}M_xSn$ (M=Sc,V) was synthesized as described above (see Sec. III). The crystal structure of the samples was investigated by powder XRD using excitation by Mo $K\alpha$ radiation. Figure 5 shows the obtained diffraction pattern of the compound NiTiSn as an example. All compounds exhibit the $C1_b$ structure. The Rietveld refinement for a disorder of 5% swapped Ti to the vacant position (Vc) delivered the lowest R values. The difference to the measured data is shown in Fig. 5. The refinement of the data resulted in a lattice parameter of a =5.9185 Å for pure NiTiSn. This value agrees with the values found in literature.[6,33] The inset in Fig. 5 shows a monotonic increase in the lattice parameter of $NiTi_{1-x}Sc_xSn$ with increase in the scandium content. A linear regression gives a slope of $\Delta a = x \times 2.54 \times 10^{-3}$ Å. This increase is caused when replacing the Ti atoms of smaller size (r_{Ti}=1.36 Å) by the larger Sc atoms (r_{Sc}=1.44 Å). The dependence of the lattice parameter of the V (r_V=1.25 Å) substituted compounds exhibits only a very low decrease (not shown here).

1. Hard x-ray photoelectron spectroscopy

The electronic structure of the series $NiTi_{1-x}Sc_xSn$ was investigated by HAXPES. Figure 6 compares the measured

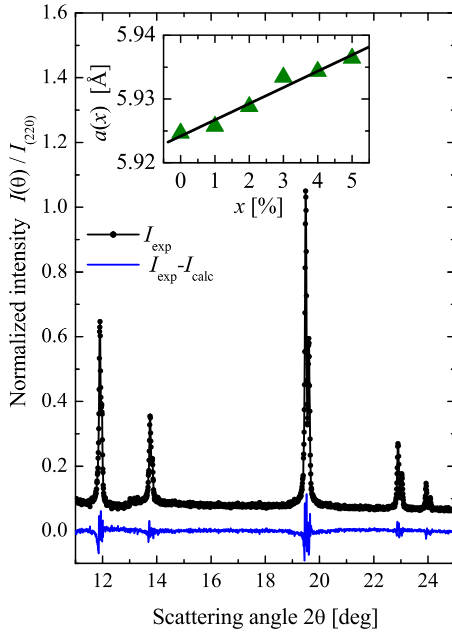

FIG. 5. (Color online) X-ray diffraction of polycrystalline NiTiSn. The data were taken at room temperature using Mo $K\alpha$ radiation. The inset shows the dependence of lattice parameter a for $NiTi_{1-x}Sc_xSn$ versus Sc content. The line is a result of a linear fit to Vegards law.

valence-band spectra of NiTiSn to the Sc-substituted compounds $NiTi_{1-x}Sc_xSn$. The spectra were taken at 20 K with an excitation energy of about 7.9 keV. The low-lying $a_1(s)$ states are revealed below −7.5 eV as well as the sp hybridization gap being typical for Heusler compounds. The higher lying valence-band spectrum of NiTiSn shows clearly a structure with four major peaks at energies of about −1.3 eV, −2.3 eV, −3.1 eV, and −4.9 eV below the Fermi energy (ϵ_F) that are associated with p and d states, in agreement to the calculated density of states. Compared to the electronic-structure calculations the peaks arise mainly from $t_1(p)$ states (−4.9 eV), t_2 states (−3.1 eV) as well as unresolved e and t_2 states (−2.3 eV) located at the Ni atoms, and of different d states located at Ni and Ti (−1.3 eV). The

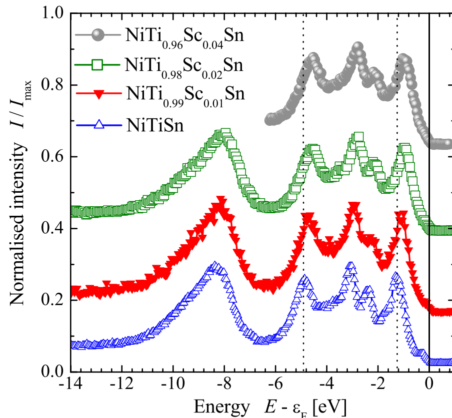

FIG. 6. (Color online) Valence-band spectra of $NiTi_{1-x}Sc_xSn$ (x=0, 0.01, 0.02, and 0.04). The measurements were performed at 20 K, the excitation energy was fixed to 7.939 keV.

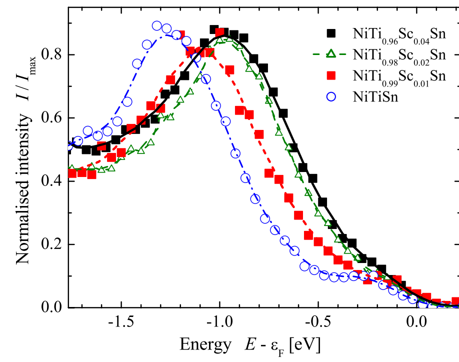

FIG. 7. (Color online) Valence-band spectra of $NiTi_{1-x}Sc_xSn$ close to the Fermi edge ϵ_F for an excitation energy of 7.939 keV and an improved, higher resolution (ΔE=150 meV) compared to Fig. 6.

states with different symmetry characters are not resolved in the spectra. Similar structures are also observed for the Sc-substituted compounds. A remarkable shift of the peaks toward the Fermi edge is obtained with increase in the Sc content. It is explained by the depletion of states in the valence band when substituting Ti ($3d^2 4s^2$) by Sc ($3d^1 4s^2$). As a fact, the Fermi energy is lowered or—equivalently—the bands move toward ϵ_F that is here the reference energy.

Figure 7 compares the valence-band spectra close to the Fermi energy that were taken with a higher energy resolution. For the pure NiTiSn compound one observes typical in gap states. These states were previously suggested to be responsible for the excellent thermoelectric properties of such compounds,[14] and make the pure compound metallic as shown in the calculations. The shape of the observed in gap states corresponds well to the assumption of a Ni↔vacancy swap as will be discussed below. The area of the in-gap states is about 0.5% of the overall valence-band spectrum. Assuming constant and equal cross sections for all states this would correspond to about 0.1 electrons only. Figure 7 reveals also the shift of the states toward ϵ_F while increasing the amount of Sc. The observed shift is not linear for two reasons. The Sc substitution does not decrease linearly the numbers of states at ϵ_F [see inset in Fig. 11(a)] and moreover it suppresses the in-gap states.

As found by powder XRD (see above), the pure NiTiSn tends to antisite disorder with Ti swapped into the vacant position of the $C1_b$ lattice. The KKR method in conjunction with coherent potential approximation was used to investigate the changes in the electronic structure for different types of disorders. Figure 8 compares the consequences of different types of disorders on the density of states. Assumed is a swapping of the atoms from their regular sites to the vacant position (Vc) of the $C1_b$ structure without changing the overall composition. States appear in the band gap and NiTiSn becomes metallic in all three cases already if 1% of the atoms is exchanged with the vacancy. The details of the changes in the density of states inside of the initial band gap are rather different for the three types of atoms. For Ni an additional state appears at ϵ_F close to the middle of the original gap whereas several states are obtained for Sn. In all three cases the total energy (about 17.1×10^3 Ry) of the sys-

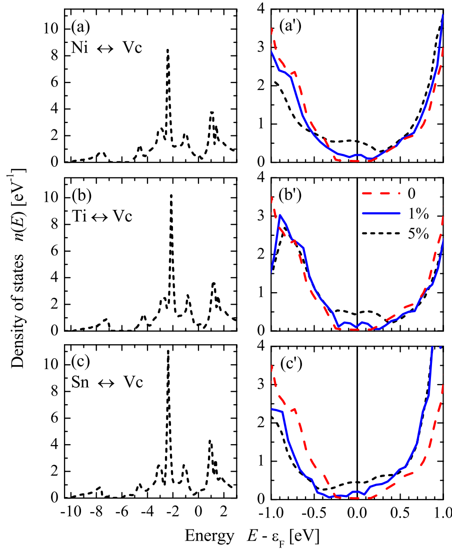

FIG. 8. (Color online) Density of states of disordered NiTiSn. The left panels (a)–(c) show the density of states for 5% of the atoms swapped into the vacant site (Vc). The right panels (a′)–(c′) compare the part around the Fermi energy for different amounts of disorder to the well-ordered compound. The Fermi energy (ϵ_F) of ordered NiTiSn was placed in the middle of the band gap for better comparison.

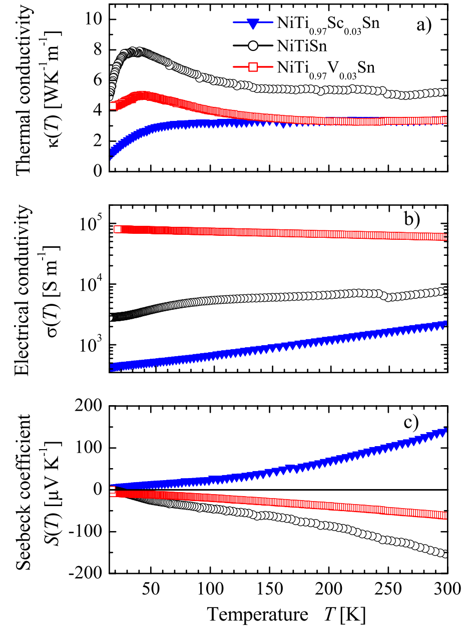

FIG. 9. (Color online) Temperature dependence of thermal conductivity $\kappa(T)$, electrical conductivity $\sigma(T)$, and Seebeck coefficient $S(T)$ of NiTiSn and $NiTi_{0.97}M_{0.03}Sn$ (M=Sc,V).

tem becomes slightly higher with the disorder and increases with the amount of disorder (assuming an unchanged lattice parameter). For Ni↔Vc the energy of the disordered state is about 0.5 Ry higher at a disorder level of 1% (2.5 Ry at 5%). Therefore, this type of disorder becomes very improbable. The situation is different for Ti↔Vc that raises the total energy only by about 5 mRy at 1% disorder. The Ti swap causes two impurity states at about −0.2 eV and +0.1 eV with respect to ϵ_F. At the low-disorder level the occupied state contains about 0.03 electrons (≈0.15 electrons at 5%). This type of disorder is thus consistent with the observations by XRD as well as photoelectron spectroscopy. It leads to a self-doping in the compound and finally in a high n-type Seebeck coefficient as will be shown in the following.

Independent of the type of disorder, the in gap states always make the compound metallic. It is worthwhile to note that similar impurity states will appear if the substituted elements occupy the vacant sites instead of the original Ti position. The situation becomes more complicated because the number of valence electrons is changed at the same time.

2. Transport properties

The measured temperature dependence of the transport properties for different types of substitutions (Sc, V) are shown in Fig. 9 for three exemplary cases. Figure 9 compares the temperature dependence of electrical conductivity $\sigma(T)$, thermal conductivity $\kappa(T)$, and Seebeck coefficient $S(T)$ of pure NiTiSn to the substituted compounds $NiTi_{0.97}Sc_{0.03}Sn$ and $NiTi_{0.97}V_{0.03}Sn$. The pure compound does not exhibit a clear semiconducting behavior what is expected from the occurrence of the in-gap states reported above. Substituting Ti by V makes the compound metallic with a typical decreased electrical conductivity by increasing of the temperature. On the other hand, the values of the electrical conductivity is changed by more than one order of magnitude in comparison with that of the nondoped compound. It stays increasing with temperature under Sc substitution, what gives another hint on the suppression of the in gap states.

The thermal conductivity $\kappa(T)$ of NiTiSn exhibits a maximum at about 30 K that is typical for well-ordered compounds. Substituting Ti by Sc or V results in a considerably lower thermal conductivity and in the case of Sc to a full suppression of the maximum. The decrease in $\kappa(T)$ is explained by scattering of electrons and phonons at the substituted atoms that act as impurities even though they occupy regular lattice sites. At higher temperatures, the thermal conductivity of both substituted compounds becomes nearly equal what points to similar scattering processes.

The Seebeck coefficient is already n type in the pure compound. It stays negative, as expected, but its absolute value becomes smaller when substituting Ti by V. When substituting Ti by Sc the Seebeck coefficient reverses the sign such that the compound becomes p type in full agreement with the expectations from the calculations. Most interestingly, the Seebeck coefficient changes the sign at 300 K from −155 μV/K for the undoped compound to +140 μV/K for the compound with 3% Sc substitution.

Figure 10 compares the behavior of the measured transport properties as function of the substitution of Ti by Sc [Fig. 10(a)] or V [Fig. 10(b)] at fixed temperatures (100 and 300 K). The data for high Sc substitution with $x \geq 5\%$ reported by Romaka *et al.*[34] continue seamless the low substitution results reported here. The general variation and changes in the transport properties agree qualitatively with the calculated transport coefficients using Boltzmann trans-

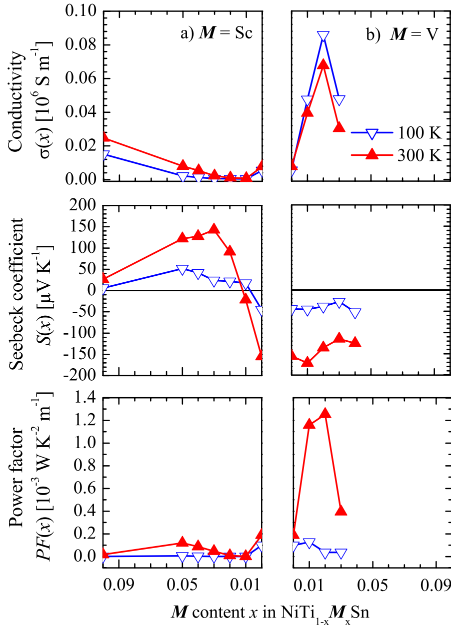

FIG. 10. (Color online) Dependence of the electric conductivity $\sigma(x)$, Seebeck coefficient $S(x)$, and power factor $PF(x)$ on the electron and hole doping of $NiTi_{1-x}M_xSn$ (M=Sc,V).

port theory (see above). Neglecting the differences observed for the pure NiTiSn compound that are caused by in-gap states, the sign and occurrence of maxima (minima) of the Seebeck coefficient are in agreement to a simple doping electrons or holes model as given in Fig. 2. The sign of the Seebeck coefficient for NiTiSn is negative and changes to positive with increasing the substitution ratio on Sc. Since the number of valence electrons of Sc is one less than that of Ti, Sc acts as a hole donor and the number of hole carries increases. The absolute value of the Seebeck coefficient decreases with increasing amount of V. The electron doping increases the density of states at ϵ_F due to the Fermi-level shift to a higher position in the conduction band (Fig. 4). As a result, the Seebeck coefficient decreases with V concentration. The behavior agrees roughly with the result of the Boltzmann transport calculations (see Fig. 2).

Details of the observed transport properties are different from those found from Boltzmann transport equations because the latter do not contain detailed information about the relaxation times. Therefore, the residual resistivities of the substituted compounds were also calculated by means of the KKR-CPA method. The behavior of the residual resistivity due to chemical disorder is different when substituting Ti by Sc or V. In Fig. 11 the calculated conductivity $\sigma=1/\rho$ is shown that allows a better estimation of its influence on the power factor that depends linearly on σ but is inversely proportional to ρ. Compared is the calculated conductivity $\sigma(x)$ as a function of the substitution level x. The shift of the Fermi energy into the valence or conduction band (see Fig. 4) makes the compound metallic. The resulting increase in the density of states at the Fermi energy is obvious from the insets in Fig. 11. Its progression is different for Sc or V because of the differences in the valence or conduction bands, respectively. The results for Sc substitution agree well

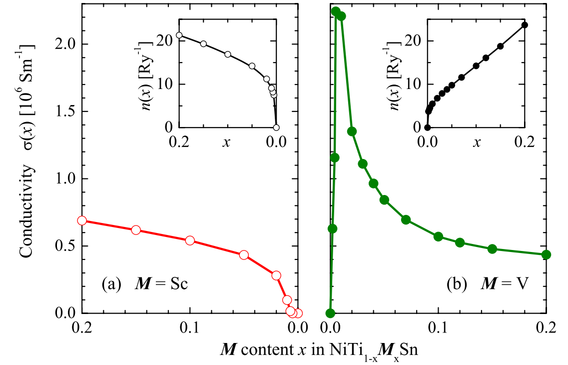

FIG. 11. (Color online) Calculated conductivity of M=Sc- and V-substituted $NiTi_{1-x}M_xSn$. (a) shows the results of Sc↔Ti and (b) of V↔Ti substitution corresponding to hole or electron doping, respectively. The insets show the density of states $n(\epsilon_F,x)$ at the Fermi energy as function of the substitution. The density of states was broadened by a Lorentzian to reduce the numerical noise.

with those reported by Stopa *et al.*[35] The conductivity behaves quite different for the two kinds of substitution, even though the general increase in $n(\epsilon_F,x)$ is rather similar without large differences in its magnitude (see insets in Fig. 11). For the case of Ti substitution by Sc, $\sigma(x)$ reflects directly the increase in the number of electrons that take part in the transport properties. The initial increase in $\sigma(x)$ is much more pronounced for V caused by the different characters of the conduction band compared to the valence band (see also Fig. 1), already at 0.2% substitution the compound becomes metallic. The conductivity exhibits a maximum at about 1% substitution of Ti by V. The following decrease in $\sigma(x)$ is explained by the increase in chemical-disorder scattering at the V atoms. In contrast to Sc substitution, the increase in the V impurity scattering is not compensated by the increase in $n(\epsilon_F,x)$ with increasing x.

The details reveal that a simple shift of the chemical potential is not able to explain the measured data. For the power factor, that does contain the scattering rates, this is easily understandable. Obviously, the calculation of the Seebeck coefficient needs also the inclusion of different scattering rates for different bands rather than a single, fixed relaxation time. The differences between Sc- and V-type substitutions are obvious from the band structure of the pure NiTiSn compound. From Fig. 1 it is easily seen that p-type doping (Sc) creates holes in the triply degenerate (at Γ) topmost valence band. The situation is completely different for n-type doping (V) where only the single state of the lowest conduction band above the indirect gap at X is filled by electrons. The difference in the relaxation times for electrons in the various involved bands together with the different characters of those bands have finally the effect that the behavior of the power factor does not agree with the prediction shown in Fig. 2.

The measured conductivity agrees well with the Kubo-Greenwood-type calculations that account for chemical disorder, not only qualitatively but also quantitatively if keeping in mind that the calculated values represent the residual resistivity for 0 K. Obviously the disorder scattering causes completely different results if the electrons responsible for

the transport are from the "initial valence" band for Sc substitution or the "initial conduction" band for V substitution. The behavior of the conductivity has a major impact on the behavior of the power factor under substitution. The highest value is observed for the *n*-type V substitution and the *p*-type Sc substitution leads to considerably lower power factors. Indeed, the difference arises from the different behavior of the conductivity for both types of substitutions. It is worthwhile to note that the rather comparable impact of the substitution on the thermal conductivity favors a high figure of merit for the *n*-type material. According to this observation, the improvement of *p*-type materials needs essentially an improvement of their electric conductivity and thus of their power factor.

V. SUMMARY

The solid-solution series $NiTi_{1-x}M_xSn$ (M=Sc,V) was systematically studied by experimental and theoretical methods. The electronic structure and transport properties of the compounds were measured in detail and compared to all-electron *ab initio* density-functional calculations. The results show the possibility to create *n*-type and *p*-type thermoelectric materials within one compound series.

X-ray powder diffraction was performed to determine the structure type and the lattice parameters of the compounds. All compounds of the series crystallize in the $C1_b$ structure type. Substitution of Ti by V or Sc leads to a linear change in the lattice parameter according to Vegards law. A swap of about 5% Ti into the vacant site was found from the diffraction data of pure NiTiSn. Calculations as well as photoelectron spectroscopy revealed that this type of antisite disorder is responsible for the occurrence of in gap states that result in the favorable thermoelectric properties of the pure compound.

The thermal conductivity, electrical resistivity, and Seebeck coefficient were measured in the temperature range from 10 to 300 K. In general the change in measured transport properties with composition agree qualitatively with the calculations. The *n*-type behavior of the pure compound is provided by the in gap states. Sc substitution of Ti leads to a *p*-type behavior and a suppression of the in gap states. The observed behavior of the resistivity of both types of substituted materials is explained by the calculations respecting disorder scattering. The lattice thermal conductivity of the $NiTi_{1-x}M_xSn$ (M=Sc,V) compounds are effectively depressed by substitution of Ti by Sc or V. The sign of the Seebeck coefficient with Sc substitution from *n* to *p* type is related to the appearance and the dominant contribution of free holes to the intermetallic semiconductor conductivity. In addition, the electronic structure of the compounds was studied using bulk sensitive, hard x-ray photoelectron spectroscopy. The observed in gap states suggested that the electronic states close to the Fermi edge play a key role to control the thermoelectric properties. The observed shifts of the valence states agree with the calculated shift of the Fermi energy when substituting Ti by Sc or V.

The reduction in the thermal conductivity is achieved by substitution of Ti and independent of the type of the doping (Sc or V). Therefore, the impact of the lowered thermal conductivity on the figure of merit is nearly the same. In order to create high efficient thermoelectric materials, it is necessary not only to improve the figure of merit but also to achieve a high power factor. The power factors found in calculation and experiment reveal clearly a different behavior for both types of substitutions. Different from *n*-type substitution, which exhibits the highest power factor, the *p* type still has rather low values. This difference is caused by the different behavior of the conductivity when the carriers are from either the valence or the conduction band. The major distinction appears through the fact that *p*-type doping (Sc) creates holes in the triply degenerate valence band at Γ whereas *n*-type doping (V) fills electrons in the single conduction band above the indirect gap at *X*. This behavior is typical for the semiconducting transition-metal-based Heusler compounds with $C1_b$ structure that all exhibit similar band structures rather independent of the composition.

Respectively, the open challenge to theory and experiment is to find new concepts that depress the thermal conductivity and, at the same time, improve the conductivity at low *p*-type doping of Heusler compounds. The presented systematic study of the solid-solution series $NiTi_{1-x}M_xSn$ (M=Sc,V) shows the possibility to create *n*-type and *p*-type thermoelectric materials within one compound series.

ACKNOWLEDGMENTS

The authors gratefully acknowledge financial support by the Deutsche Forschungsgemeinschaft (Project No. FE 633/8-1) and Stiftung Rheinland Pfalz für Innovation (Project 863). The synchrotron radiation HAXPES measurement were performed at BL47XU with the approval of the Japan Synchrotron Radiation Research Institute (JASRI) (Long-term Proposal No. 2008B0017).

*fecher@uni-mainz.de

[1] W. Jeitschko, Metall. Mater. Trans. B **1**, 3159 (1970).
[2] H. C. Kandpal, C. Felser, and R. Seshadri, J. Phys. D **39**, 776 (2006).
[3] J. Tobola and J. Pierre, J. Alloys Compd. **296**, 243 (2000).
[4] J. R. Sootsman, D. Y. Chung, and M. G. Kanatzidis, Angew. Chem. **48**, 8616 (2009).
[5] S. Sakurada and N. Shutoh, Appl. Phys. Lett. **86**, 082105 (2005).
[6] N. Shutoh and S. Sakurada, J. Alloys Compd. **389**, 204 (2005).
[7] S. Katsuyama, R. Matsuo, and M. Ito, J. Alloys Compd. **428**, 262 (2007).
[8] T. Katayama, S. W. Kim, Y. Kimura, and Y. Mishima, J. Electron. Mater. **32**, 1160 (2003).

[9] Q. Shen, L. Chen, T. Goto, T. Hirai, J. Yang, G. P. Meisner, and C. Uher, Appl. Phys. Lett. **79**, 4165 (2001).

[10] J. Yang, G. P. Meisner, and L. Chen, Appl. Phys. Lett. **85**, 1140 (2004).

[11] D. Rowe, *Thermoelectrics Handbook: Macro to Nano* (CRC Taylor & Francis, Boca Raton, 2006).

[12] J. Yang, Adv. Funct. Mater. **18**, 2880 (2008).

[13] A. Horyn', O. Bodak, L. Romaka, Y. Gorelenko, A. Tkachuk, V. Davydov, and Y. Stadnyk, J. Alloys Compd. **363**, 10 (2004).

[14] K. Miyamoto, K. Kimura, K. Sakamoto, M. Ye, Y. Cui, K. Shimada, H. Namatame, M. Taniguchi, S. I. Fujimori, Y. Saitoh, E. Ikenaga, K. Kobayashi, J. Tadano, and T. Kanomata, Appl. Phys. Express **1**, 081901 (2008).

[15] P. Blaha, K. Schwarz, G. K. H. Madsen, D. Kvasnicka, and J. Luitz, *WIEN2k, An Augmented Plane Wave+Local Orbitals Program for Calculating Crystal Properties*, edited by Karlheinz Schwarz (Techn. Universität Wien, Wien, Austria, 2001).

[16] G. K. H. Madsen and D. J. Singh, Comput. Phys. Commun. **175**, 67 (2006).

[17] T. Graf, G. H. Fecher, J. Barth, J. Winterlik, and C. Felser, J. Phys. D **42**, 084003 (2009).

[18] J. Barth, G. H. Fecher, B. Balke, S. Ouardi, T. Graf, C. Felser, A. Shkabko, A. Weidenkaff, P. Klaer, H. J. Elmers, H. Yoshikawa, S. Ueda, and K. Kobayashi, Phys. Rev. B **81**, 064404 (2010).

[19] J. P. Perdew, K. Burke, and M. Ernzerhof, Phys. Rev. Lett. **77**, 3865 (1996).

[20] H. Ebert, in *Electronic Structure and Physical Properties of Solids. The Use of the LMTO Method*, Lecture Notes in Physics Vol. 535, edited by H. Dreysee (Springer-Verlag, Berlin, 1999), pp. 191–246.

[21] P. Weinberger, *Electron Scattering Theory for Ordered and Disordered Matter* (Clarendon Press, Oxford, 1990).

[22] W. H. Butler, Phys. Rev. B **31**, 3260 (1985).

[23] J. P. Perdew, A. Ruzsinszky, L. A. Constantin, J. Sun, and G. I. Csonka, J. Chem. Theory Comput. **5**, 902 (2009).

[24] E. Engel and S. H. Vosko, Phys. Rev. B **47**, 13164 (1993).

[25] A. D. Becke, J. Chem. Phys. **98**, 5648 (1993).

[26] J. P. Perdew and Y. Wang, Phys. Rev. B **45**, 13244 (1992).

[27] J. P. Perdew, A. Ruzsinszky, G. I. Csonka, O. A. Vydrov, G. E. Scuseria, L. A. Constantin, X. Zhou, and K. Burke, Phys. Rev. Lett. **100**, 136406 (2008).

[28] J. M. Ziman, *Electrons and Phonons* (Oxford University Press, Oxford, 1960).

[29] L. L. Wang, L. Miao, Z. Y. Wang, W. Wei, R. Xiong, H. J. Liu, J. Shi, and X. F. Tang, J. Appl. Phys. **105**, 013709 (2009).

[30] M. Onoue, F. Isshii, and T. Oguchi, J. Phys. Soc. Jpn. **77**, 054706 (2008).

[31] K. Kroth, B. Balke, G. H. Fecher, V. Ksenofontov, C. Felser, and H. J. Lin, Appl. Phys. Lett. **89**, 202509 (2006).

[32] B. Balke, G. H. Fecher, A. Gloskovskii, J. Barth, K. Kroth, C. Felser, R. Robert, and A. Weidenkaff, Phys. Rev. B **77**, 045209 (2008).

[33] J. Pierre, R. V. Skolozdra, Y. K. Gorelenko, and M. Kouacou, J. Magn. Magn. Mater. **134**, 95 (1994).

[34] L. Romaka, Y. Stadnyk, A. Horyn, M. Shelyapina, V. Kasperovich, D. Fruchart, E. Hlil, and P. Wolfers, J. Alloys Compd. **396**, 64 (2005).

[35] T. Stopa, J. Tobola, S. Kaprzyk, E. Hlil, and D. Fruchart, J. Phys.: Condens. Matter **18**, 6379 (2006).